

Toward Clean Suspended CVD Graphene

Alexander Yulaev^{1,2,3}, Guangjun Cheng⁴, Angela R. Hight Walker⁴, Ivan V. Vlassiouk⁵, Alline Myers¹, Marina S. Leite^{2,6}, and Andrei Kolmakov^{1*}*

¹Center for Nanoscale Science and Technology, NIST, Gaithersburg, MD 20899, USA;

²Department of Materials Science and Engineering, University of Maryland, College Park, MD 20742, USA;

³Maryland NanoCenter, University of Maryland, College Park, MD 20742, USA;

⁴Physical Measurement Laboratory, NIST, Gaithersburg, MD 20899, USA;

⁵Oak Ridge National Laboratory, Oak Ridge, TN 37831, USA;

⁶Institute for Research in Electronics and Applied Physics, University of Maryland, College Park 20742, USA

Keywords: graphene transfer, anthracene, purity, scanning electron microscopy

*To whom correspondence should be sent: andrei.kolmakov@nist.gov; mleite@umd.edu

Abstract

The application of suspended graphene as electron transparent supporting media in electron microscopy, vacuum electronics, and micromechanical devices requires the least destructive and maximally clean transfer from their original growth substrate to the target of interest. Here, we use thermally evaporated anthracene films as the sacrificial layer for graphene transfer onto an arbitrary substrate. We show that clean suspended graphene can be achieved *via* desorbing the anthracene layer at temperatures in the 100 °C to 150 °C range, followed by two sequential annealing steps for the final cleaning, using Pt catalyst and activated carbon. The cleanliness of the suspended graphene membranes was analyzed employing the high surface sensitivity of low energy scanning electron microscopy and x-ray photoelectron spectroscopy. A quantitative comparison with two other commonly used transfer methods revealed the superiority of the anthracene approach to obtain larger area of clean, suspended CVD graphene. Our graphene transfer method based on anthracene

paves the way for integrating cleaner graphene in various types of complex devices, including the ones that are heat and humidity sensitive.

Introduction

Ultra-thin and clean suspended graphene (Gr) membranes have been applied in a variety of micromechanical devices,¹ sensors,² and vacuum electronics;³ as supporting media for high-resolution transmission electron microscopy (HRTEM),⁴ and as electron transparent windows in ambient pressure photoelectron spectroscopy and microscopy.⁵ The mechanical exfoliation of the graphite flakes remains to be the cleanest method to prepare such devices but it is low yield and labor intensive. Alternatively, ultrathin membranes assembled of interlocked chemically exfoliated graphene (graphene oxide) flakes or platelets are simple to fabricate⁶, however, they possess a large amount of defects and reactive functional groups. The latter, being advantageous for the development of new composite materials⁷ *via* graphene functionalization, can lead to undesirable alteration of the physical and chemical properties of the membrane devices. On the other hand, the growth of graphene *via* chemical vapor deposition (CVD) on copper or nickel substrates is a well-developed, large-scale, and high-yield method of graphene production with large single crystal domain size.⁸ In order to transfer graphene from copper or nickel foils onto a target substrate, multiple approaches have been implemented, which can be roughly classified into two groups: “wet” and “dry” methods, depending on whether any liquid is involved during the final stage of the graphene layer transfer. For suspended graphene devices, wet transfer methods *via* a sacrificial layer⁹⁻¹¹ or direct transfer approaches using capillary action of solvent droplets¹² (*e.g.* isopropyl alcohol (IPA)) as an adhesion promoter are commonly used. The former method usually relies on a polymethyl methacrylate (PMMA) layer spin-coated over the Gr-metal substrate, followed by etching of the metal and transferring the PMMA/Gr onto a target substrate.

After the transfer, the PMMA layer is dissolved in solvents, or removed by annealing in vacuum¹³ or under reducing conditions.¹⁴ Recently, alternative polymer scaffolds have been used instead of PMMA, which do not require an additional annealing after the polymers are dissolved.¹⁵ However, some of the copper etchants, such as ammonium persulfate, can promote a crosslinking in polymers, resulting in a high concentration of residues on the graphene layer.¹⁶ Alternatively, the direct transfer method is based on an adhesion between a Gr/substrate stack and a flexible perforated carbon membrane induced by capillary forces of a drying solvent such as IPA.¹² In this case, the growth substrate is etched away, and, after rinsing in water and drying, a suspended, high-quality membrane is obtained. Other wet methods of graphene transfer include the soak-and-peel,¹⁷ bubbling transfer,¹⁸ and electrochemical delamination (see Refs.¹⁹⁻²¹ for a detailed description of each approach).

Dry transfer of graphene is necessary when the target substrate is reactive or sensitive to moisture. Solvent-free methods to transfer CVD-grown Gr employ polydimethylsiloxane (PDMS) stamps,²² thermal release tape,²³ thermal decomposition of PMMA in forming gas⁹, etc.

The application of graphene in electron or scanning probe microscopies, in microelectromechanical systems (MEMS) / electronic devices and many other fields requires the ultimate surface cleanliness of the suspended membrane. However, all the aforementioned transfer methods unavoidably contaminate the graphene surface, requiring a sequential step of rigorous cleaning. The direct comparison of the reported cleaning methods is hard to conduct due to the variety of transfer conditions and characterization techniques used. Therefore, a systematic and quantitative comparison of the most commonly used methods is essential to determine the most effective one.

Here, we demonstrate a novel ultraclean method for the transfer of CVD-grown graphene utilizing an anthracene film as a sacrificial layer. Different from higher molecular mass polycyclic aromatic hydrocarbons (PAHs) which strongly interact with graphene, an anthracene film can easily sublime at moderate temperature ($< 150\text{ }^{\circ}\text{C}$),²⁴ thus preventing structural changes of the graphene and a sensitive target substrate. We also perform a comparative cleanliness analysis of our approach with two widely used transfer methods: (i) direct transfer by IPA¹² and (ii) PMMA-based transfer.⁹ The samples transferred *via* all three aforementioned protocols were subjected to the same two step cleaning procedure after the transfer: annealing in the presence of platinum catalyst²⁵ followed by annealing in activated carbon.²⁶ The cleanliness of the resultant membranes was examined with techniques highly sensitive to the surface contamination and defects: low-voltage (1 keV) scanning electron microscopy (LVSEM), x-ray photoelectron spectroscopy (XPS), and transmission electron microscopy (TEM). We show that graphene transferred by anthracene is consistently cleaner and less defective than samples prepared using other methods

Experimental procedures

Sample preparation and transfer using anthracene

Graphene was grown from a methane gas precursor on a copper substrate using the standard CVD method, which is described in details elsewhere^{8,27,28}. Briefly, electropolished in phosphoric acid 125 μm thick copper foils were loaded into atmospheric pressure CVD reactor and annealed at 1065 C under the flow of 2.5% H₂ in Ar for 30 min. Graphene growth was performed by addition of methane with a gradual increase of concentration from 10 to 20 to 40 ppm for 30 min increments. After cooling down to room temperature, a monolayer of graphene with less than 5 % fraction of the hexagon-shaped bilayer was formed on both sides of the copper foil.

An anthracene film with an average thickness of $14 \mu\text{m} \pm 7 \mu\text{m}$ was thermally evaporated onto as-grown graphene on a copper foil in vacuum ($\approx 10^{-3}$ Pa) (Figure 1a, (ii)). Dense and mechanically stable, quasi-amorphous films were obtained if the deposition was conducted onto a pre-cooled (≈ -20 °C) Gr/substrate in vacuum. Note that low temperature of a substrate is essential to increase the density of the nucleation sites for anthracene (Figure S1). After the deposition onto the pre-cooled sample (Figure 1a, (ii)), the copper substrate was etched in aqueous ammonium persulfate solution (APS) (Figure 1a, (iii)). The Gr-anthracene stack was then rinsed in distilled water, and transferred directly to the TEM mesh for inspection (Figure 1a, (iv)). After annealing at 120 °C for 40 min (Figure 1a, (v)), the anthracene film sublimed, and only the graphene layer was left on the target substrate (Figure 1a, (vi)). Besides the low temperature sublimation of anthracene, the other advantage of this PAH is its high fluorescence yield under ultraviolet (UV) light irradiation (Figures 1b, 1c), which helps visualize the anthracene during the transfer process and track residues left on graphene after annealing (Figures 1b, 1c).

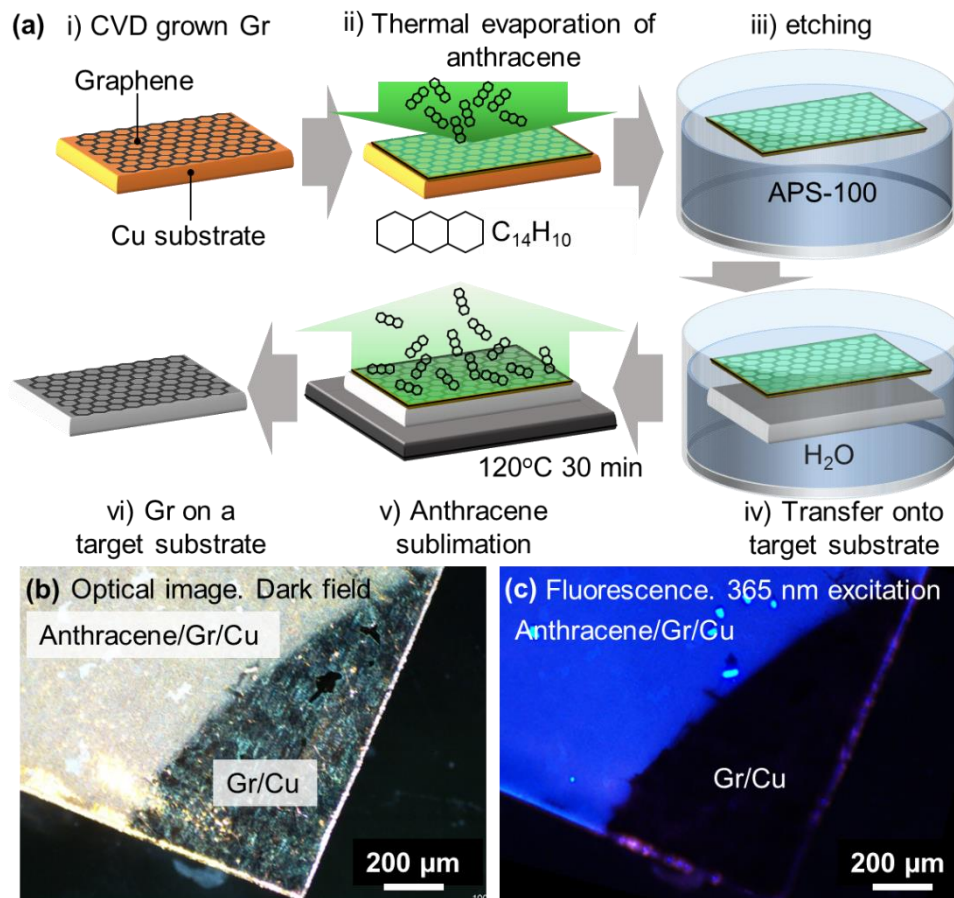


Figure 1. Graphene transfer by anthracene. (a) Illustration of the transfer procedure: (i) CVD-grown graphene on a copper substrate; (ii) thermal evaporation of anthracene onto graphene at ≈ -20 °C; (iii) copper substrate etching by aqueous solution of ammonium persulfate (APS-100) at 40 °C; (iv) Gr-anthracene transfer onto the TEM grid; (v) anthracene sublimation on a hot plate at 120 °C; (vi) graphene on a target substrate. (b) Dark field optical image of a typical anthracene film evaporated onto Gr/copper after step (ii). The dark area of the sample corresponds to pristine Gr on copper. (c) Fluorescent microscopy image of the same region shown in (b) excited using UV light-emitting diode (LED) with emission band at ≈ 365 nm.

Comparative analysis

Three sets of graphene membrane samples transferred using (i) PMMA as a sacrificial layer, (ii) IPA droplet capillary adhesion (so called “direct transfer”), and (iii) anthracene as a sacrificial layer were subjected to the same set of cleaning treatments and characterizations to compare and identify the least contaminated product.

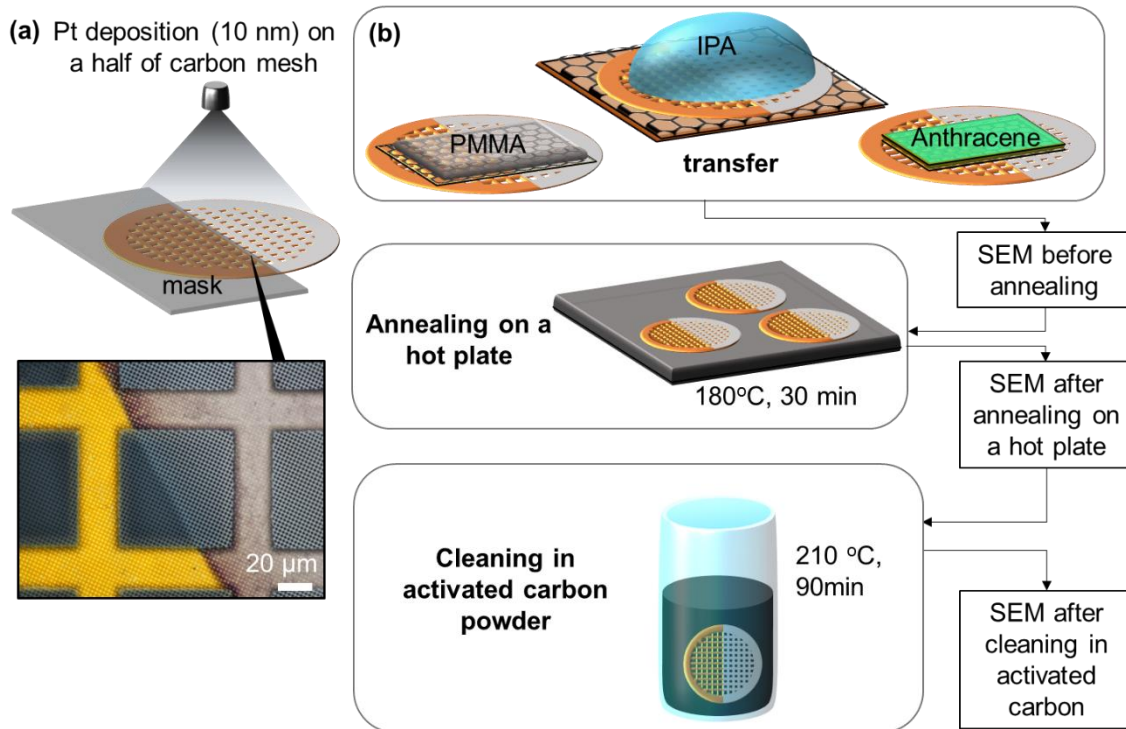


Figure 2. Sample preparation for graphene transfer methods comparison. (a) Pt deposition (10 nm) on a half of a carbon mesh (e.g. TEM grid). (b) Schematic of graphene transfer and subsequent cleaning procedure. After each step the sample was characterized by SEM.

The sample fabrication for the comparative analysis is schematically illustrated in Figure 2. First, TEM grids made of gold with a perforated, 20 nm thick carbon mesh (2 μm hole diameter) were half-coated with a 10 nm platinum layer to compare the effect of the platinum catalysis on the surface purity (Figure 2a) on the same substrate. Second, CVD-Gr films were transferred onto the grids using the three methods depicted in Figure 2b. All the samples concurrently underwent first the catalytic cleaning (180 °C, 30 min) on a hot plate in ambient air, followed by an activated carbon cleaning procedure step (210 °C, 90 min, rate 5 °C/min) in an oven. We used LVSEM to image all samples immediately as transferred, after the platinum-catalysis treatment, and, ultimately, after the cleaning in activated carbon. For LVSEM imaging, all samples have been mounted on a graphite specimen stub to minimize the background signal formed by spurious

secondary electrons. The same contrast/brightness adjustments were maintained during all three LVSEM sessions to quantitatively compare results of each cleaning step. To maximize surface sensitivity of the SEM to impurities, a low-energy electron beam (1 keV) in combination with through-the-lens secondary electrons detector, and short working distance (3 mm) were used. All samples have been studied by TEM at 300 keV electron beam energy.

XPS spectra of graphene samples were collected at $\approx 3 \times 10^{-7}$ Pa in ultra-high vacuum (UHV) chamber equipped with a 125 mm radius hemispherical electron energy analyzer operating with an emission angle of 54° . The monochromatic Al K α (1486.6 eV) X-ray source was used for the XPS measurements. The analyzer was working at the constant pass energy $E_p = 13.6$ eV and slit sizes offering an experimental energy resolution 0.55 eV. The XPS peaks of graphene were deconvoluted using mixed asymmetric Gaussian–Lorentzian line shapes after a Shirley background subtraction.

Results and discussion

The resulting suspended graphene obtained by the anthracene-based method demonstrates high yield of successful (with no holes) coverage over the perforated structure, ≈ 95 % (Figure S3), comparable with the best results obtained using the direct transfer by IPA drop and PMMA sacrificial layer. The quality of the as transferred graphene was evaluated using Raman spectroscopy *via* measuring relative intensity of the D-peak and G/D ratio (Figure S4). Different from commonly used high voltage (5 kV to 15 kV) SEM imaging, we employed low electron beam energies (0.5 keV to 1 keV) in combination with a true secondary electron (SE) detector to monitor the contaminants evolution upon different cleaning procedures. The enhanced electron interaction

cross-section and surface sensitivity of such imaging conditions are advantageous for discriminating between clean and contaminated regions on the Gr layer.^{29, 30}

SEM analysis

According to the semi-empirical law for the SE emission from carbon,³¹ the dependence of SE yield on electron beam energy E_{PE} has a maximum at 400 eV and decreases with electron beam energy due to the decrease of the stopping power. The dependence of SE yield δ on membrane thickness d and E_{PE} , can be evaluated³¹ as:

$$\delta = 0.5 \cdot \frac{E_{PE}}{\varepsilon} \cdot \frac{\lambda}{R \left(1 - e^{-\frac{d}{\lambda}}\right)},$$

where ε , λ , and R stand for the effective energy to produce SE, the effective SE escape depth, and the penetration depth of the incident electron, respectively. For a carbon membrane with $\varepsilon = 80$ eV,³¹ $\lambda = 2.5$ nm, and $R = 7$ nm, the formula yields $\delta = 0.1, 0.2,$ and 0.3 for 1, 2, and 3 layer thick graphene, respectively, implying that a clean, suspended, single Gr layer will be distinguishable from any additional carbon-containing residual layers. For our experiments we used 1 keV electron beam energy to reduce electron induced carbon contamination.

Figure 3 demonstrates the effectiveness of low-voltage SEM (LVSEM) to evaluate the cleanliness of suspended membrane. The panel (a) in Figure 3 depicts the model consisting of 20 nm thick carbon mesh covered with 10 nm Pt and one layer of graphene as in the real sample. Four carbon pads of 1, 2, 5, and 10 layer thicknesses and an open orifice mimic different levels of contamination and a tear in graphene layer, respectively. Figure 3(b) shows the corresponding Monte Carlo simulated³² SE images, where the grayscale refers to the number of SEs collected per 1000 primary electrons. According to the simulation, the impurity pads are clearly distinguishable from a pristine single-layer graphene if a low energy (<1 keV) primary electron beam is used as

the SE yield increases with impurity thickness. The experimental results qualitatively corroborate with our simulations (Figure 3c, d). As the energy of the electron beam increases from 1 keV to 3 keV, the overall SE yield from the membrane diminishes due to the reduction in the inelastic interaction cross-section. As a result, the contrast between clean, contaminated graphene and void areas decreases (Figure 3e) and the carbon membrane appears to be more transparent and cleaner.

LVSEM images of suspended graphene on a perforated carbon film with Pt (10 nm) film transferred using PMMA (top: a, b, c), IPA (center: d, e, f), and an anthracene sacrificial layer (bottom: g, h, i) are shown in Figure 4. All samples demonstrate visible contamination before cleaning, which is noted as bright spots and lighter color corrugated regions. In the case of PMMA, the typical residues are left from incomplete scission of PMMA bonds during cleaning steps.¹⁶

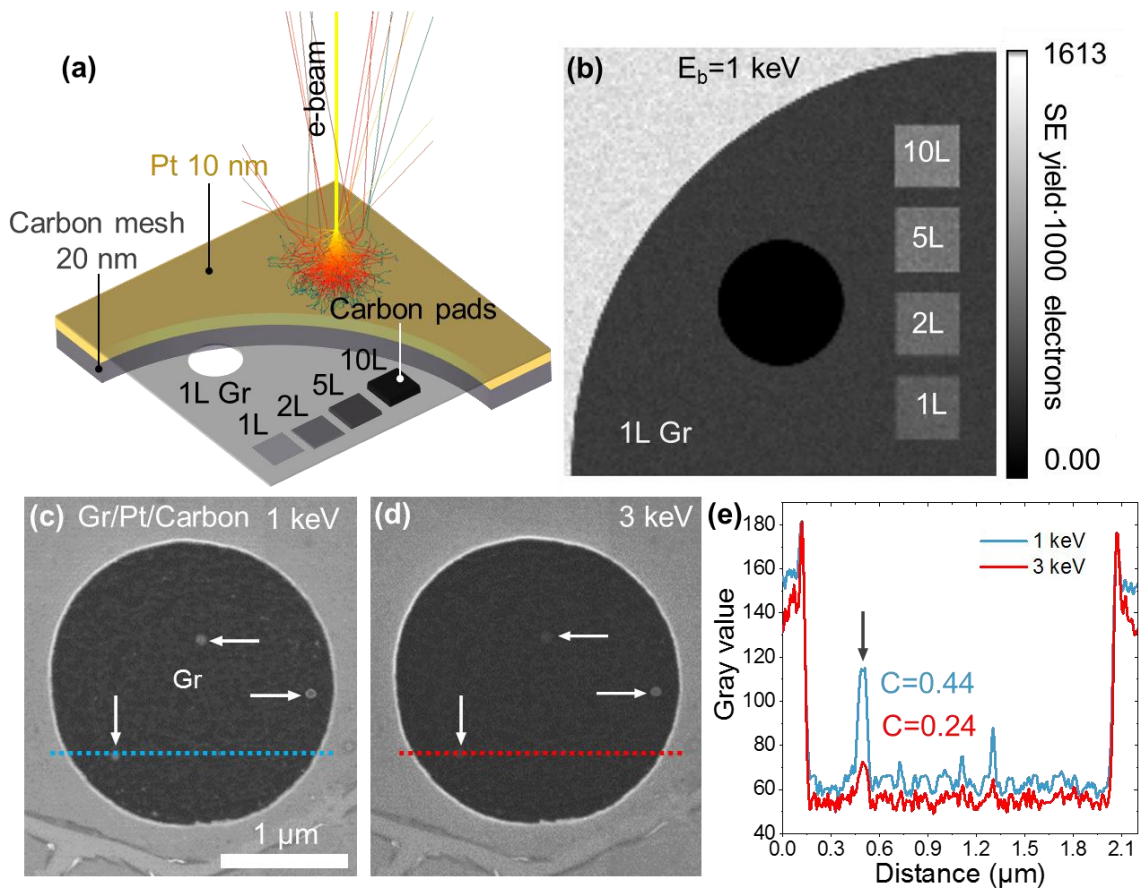


Figure 3. LVSEM imaging of suspended graphene with impurities. (a) Schematic of model used for Monte Carlo electron trajectory simulations. (b) Simulated secondary electron (SE) image of suspended graphene with overlaying carbon pads of 1, 2, 5, and 10 layer (L) thickness, mimicking impurities on the membrane. The black orifice represents void area. Gray scale bar values correspond to SE yield per 1000 primary electrons. Experimental LVSEM images of suspended graphene obtained at 1 keV (c) and 3 keV (d) energies of primary electrons. White arrows show impurities on the membrane. (e) The line profiles taken along the dotted horizontal lines in (c) and (d). Black arrow points to the same impurity visible in the panels (c) and (d). C-numbers correspond to contrast values between the impurity and graphene region calculated for images (c) and (d), respectively.

Contamination of graphene transferred by anthracene and IPA methods is mainly due to hydrocarbons; in particular, (-CH₂-) and (-CH₃) groups of hydrocarbons accumulated on the surface have been routinely detected after samples were exposed to air.³³

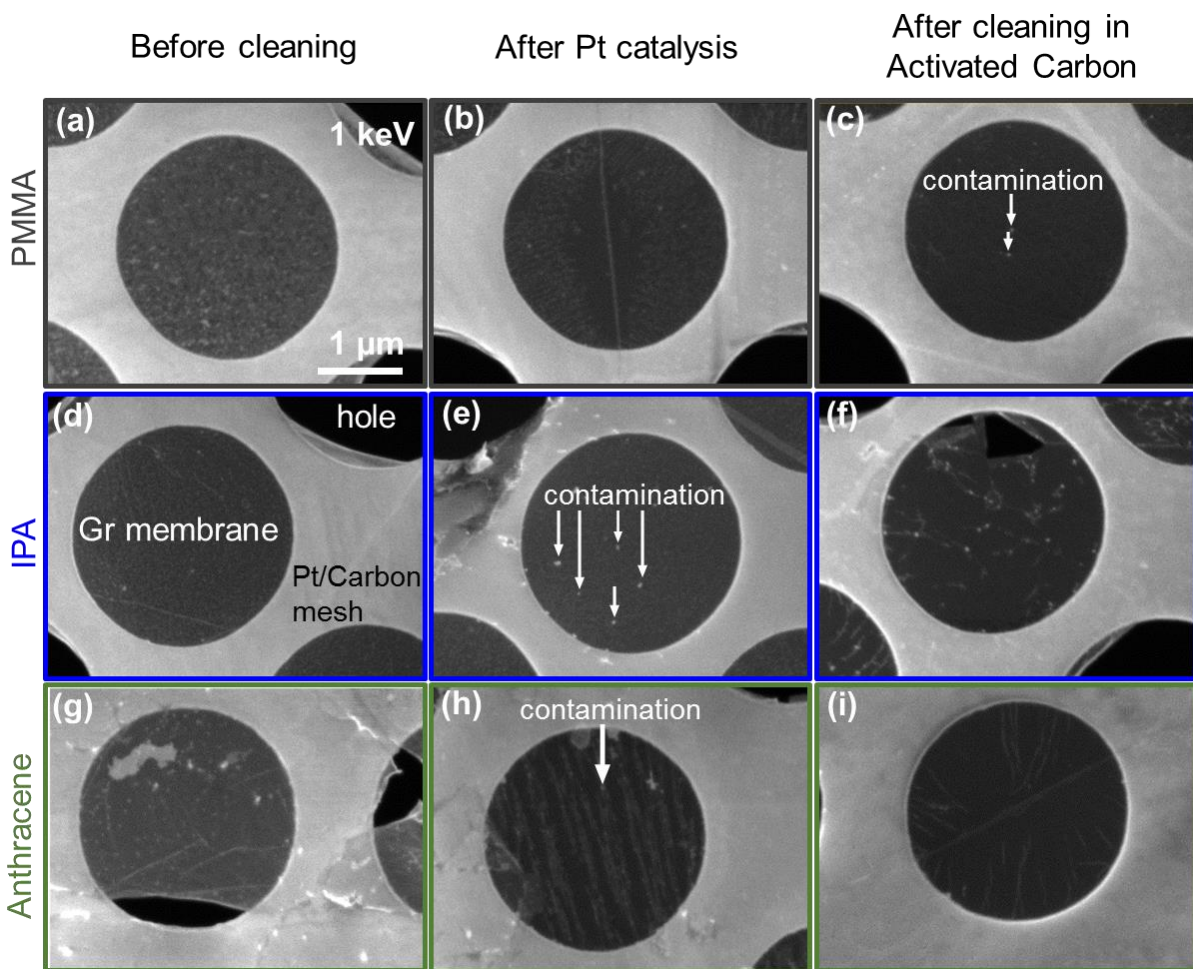


Figure 4. Comparison of the graphene cleanliness after consecutive cleaning cycles. SEM images of free-standing graphene transferred by (a, b, c) PMMA, (d, e, f) IPA, and (g, h, i)

anthracene before (left column), after annealing over Pt catalyst (central column), and after annealing in activated carbon (right column). To preserve the brightness/contrast settings, the SEM detector was set to the same fixed values of gain and offset for all the measurements.

A comparison between the different transfer methods was performed by imaging samples after each sequential cleaning step by SEM, see Figure 4. The images in the left, central, and right columns show suspended graphene before cleaning, after Pt catalytic cleaning at 180 °C, and then annealing in activated carbon, respectively. Each image contains the regions with a suspended membrane (dark circle in the center), graphene over Pt-covered carbon mesh (peripheral brightest area), and open holes (the darkest area). SEM images of moderately cleaned CVD-Gr revealed the accumulation of the contaminants in elongated strips (Figure 4b, h). The origin of such impurity distribution is attributed to stronger affinity of the impurity molecules to graphene point and extended defects,^{34, 35} as well as to wrinkles, which are common in CVD-grown graphene and occur as a result of compressive strain in as-grown carbon monolayer.³⁶ According to the set of SEM images of differently prepared samples after the aforementioned treatments, PMMA and anthracene methods demonstrate fewer residues on a carbon monolayer after two sequential cleaning steps compared to the direct transfer using IPA. The evolution of the residue concentration with a cleaning sequence can be illustrated using PMMA transferred graphene as an example. As transferred (before any additional cleaning) membrane routinely contains polymer contaminants seen as multiple bright spots and network of gray patches over the membrane (Figure 4a). The cleanliness of the suspended membranes at a microscale level can be addressed more quantitatively using the gray scale values (GSV) of SEM images, implying that the GSV is proportional to the total SE signal from the corresponding area. To conduct such measurements, the SEM detector was tuned to the same fixed values of gain and offset for entire set of measurements. The results of this analysis for all three transfer methods and samples with and

without pre-deposited Pt catalyst are summarized in Figure 5. The vertical axis values correspond to SE signal of the imaged graphene with respect to the open hole. Therefore, the cleanest and the most transparent sample will have the SE signal approaching zero.

After annealing the samples on a hot plate, the overall SE signal from all samples decreases since the large partition of the PMMA remnants become decomposed by Pt catalysis. During this process, end-chain PMMA dissociation is initiated, and the polymer degrades into monomers that can sublime.²⁵ Interestingly, the PMMA decomposition can be observed even a few microns away from the Pt catalyst (Figure S5). We assign this extended catalytic action to a spillover effect

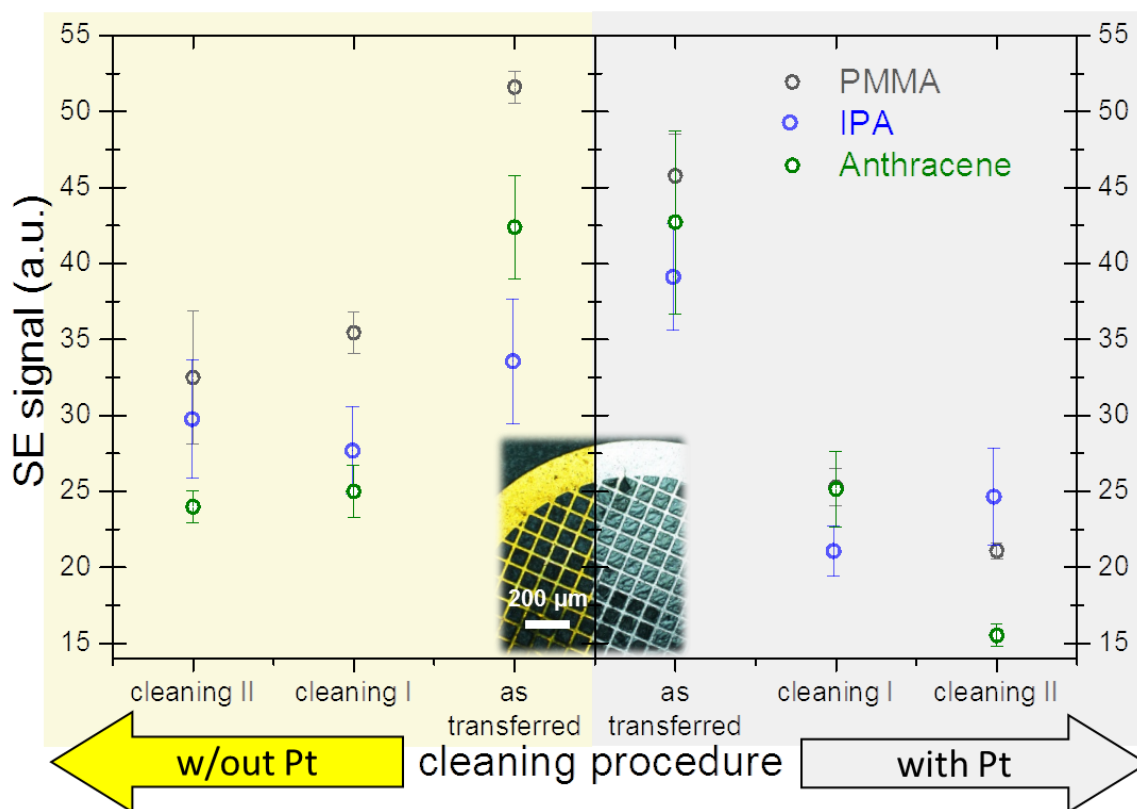


Figure 5. SE signal proportional to gray scale values of suspended graphene transferred by PMMA, IPA, and anthracene at consecutive cleaning I and II stages: annealing in presence of Pt catalyst and then annealing in activated carbon, respectively. The right panel dataset was collected from the samples in contact with Pt catalyst and the left one from platinum-free region.

Error bars represent the standard deviation value after five measurements on different sampling points.

when dissociated reactive species such as hydrogen and/or oxygen migrate from Pt to PMMA residues³⁷. As a result, the transparency of graphene after annealing in the presence of Pt catalyst increases by $\approx 50\%$ (Figure 5 right semi-plane). The electron transparency of the membrane without Pt (left semi-plane) also improves after the same treatment, however, only by $\approx 30\%$, which confirms the noticeable contribution of catalytic activation and spillover effect.

As can be seen from Figure 5 (blue dots), Pt catalysis is effective not only for PMMA decomposition, but also for cleaning of the membrane from hydrocarbon contaminants after IPA transfer. The latter results in $\approx 50\%$ cleaning effect after the treatment (compare with only $\approx 20\%$ cleaning without Pt). The similar cleaning trend can be observed for graphene transferred by anthracene yielding the cleaning effect of $\approx 50\%$ after thermal desorption of contaminants.

The cleaning effect of activated carbon with high degree of microporosity, which provides high surface area, is based on its adsorptive capacity. Upon thermal activation, the contaminants left on a graphene surface randomly diffuse until they become adsorbed and trapped by high surface area activated carbon particle. This second step of cleaning significantly improves the cleanliness of the PMMA and anthracene transferred graphene. This is not a case, though, for impurities left from IPA-based transfer. The cleaning effect is most pronounced for the sample with anthracene impurities annealed in the presence of a Pt catalyst and activated carbon. After the treatment, the transparency of the suspended membrane increased up to $\approx 65\%$ compared to as transferred graphene (Figure 5, green dots). To summarize, the combination of two aforementioned cleaning steps provides an efficient recipe to clean Gr, independent of whether PMMA or anthracene impurities were present on the sample.

It is necessary to note that electron beam induced carbon contamination can often be observed during SEM inspection of the suspended membrane.³⁸ This effect is particularly pronounced when the sample has hydrocarbon impurities and, therefore, can be used as an additional tool to evaluate graphene purity before and after the transfer. Low energy secondary electrons are mainly responsible for the dissociation of surface hydrocarbons and the buildup of the carbon deposit on a membrane.¹⁶ Interestingly, both as transferred and partially cleaned (cleaning step I, Figure 5) samples have demonstrated prominent contamination buildup during SEM imaging at room temperature after 15 s of irradiation (Figure S6). However, the carbon contamination became negligible after samples were cleaned in activated carbon, indicating that the source of the hydrocarbons are the surface residues left on samples.

XPS analysis

The microscopy results have been complemented with XPS analysis of graphene purity. For that, CVD Gr/Cu samples underwent the same set of aforementioned cleaning procedures. In particular, PMMA-covered/Gr/Cu, anthracene-covered/Gr/Cu, and IPA-immersed/Gr/Cu samples were prepared first using the standard procedures: removing the sacrificial layers by acetone, thermal sublimation, and drying, respectively. The samples then were first annealed in air (cleaning I) followed by annealing in activated carbon (cleaning II). The effective thickness of the overlay can be evaluated from the corresponding attenuation of the XPS substrate signal by carbonaceous contaminants layer.³⁹ For that, the cumulative intensity ratios of C 1s peak to attenuated Cu 2p_{3/2} peak were measured at the same spot after the sample preparation and after each cleaning procedure (Figure 6a). These data were compared to Cu 2p_{3/2} peak attenuation test of as grown and vacuum annealed pristine Gr/Cu sample considered to be ultimately clean (black square in the Figure 6a). The SESSA algorithm⁴⁰ was used to compare experimental Cu 2p_{3/2} peak

attenuation data with theoretical predictions for 1 to 4 carbon monolayers (ML) (Figure 6a). The XPS-assessed effective thickness of contaminants corroborates well with the trend observed *via* electron microscopy. In particular, as prepared samples exhibit the highest degree of contamination reaching almost four effective monolayers of impurities in the case of a PMMA-based sacrificial layer. The cleanliness of the samples improves progressively with sequential cleaning. Similar to the SEM observations above, anthracene and IPA introduced the least amount of contaminations at the graphene surface, and the final cleanliness approaches the quality of as grown and vacuum annealed CVD Gr/Cu sample, matching the theoretically predicted C 1s/Cu 2p_{3/2} ratio for 1 ML of carbon on copper.

More information on chemical nature of the contaminants can be obtained from the C 1s peak shape evolution upon the cleaning treatments. Figure 6b depicts the C 1s spectrum of as grown and vacuum annealed (10⁻⁷ Pa, 250 °C, 2 hours) Gr/Cu sample, that we consider ultimately clean graphene. The spectrum contains dominating sp² graphene component and minor

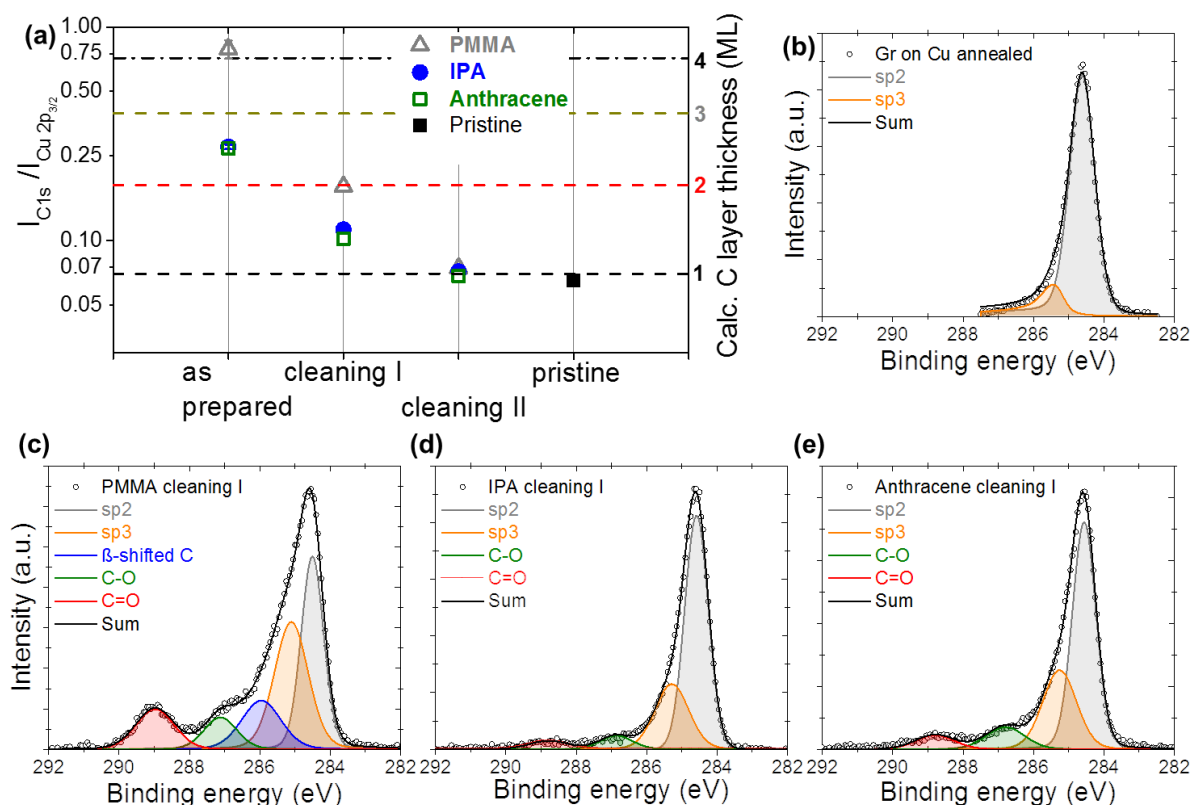


Figure 6. XPS analysis of transfer methods. (a) Ratio of C 1s peak to substrate Cu 2p_{3/2} peak for as transferred samples and after cleaning procedures for each method. Black square shows as grown and vacuum annealed pristine Gr/Cu sample. Triangle, circle, and square marks correspond to the PMMA, IPA, and anthracene samples, respectively. Error bars are smaller or comparable to the size of data marks. (b) C 1s spectrum of as grown and vacuum annealed (10⁻⁷ Pa, 250 °C, 2 hours) Gr/Cu sample. (c)-(e) XPS spectra of PMMA, IPA, and anthracene transferred samples after cleaning step I.

contribution from sp³ impurities separated by ≈ 0.75 eV. Figure 6 c-e show XPS spectra of PMMA, IPA, and anthracene transferred samples after cleaning step I. This intermediate cleaning of the PMMA sample did not completely removed a polymer as can be seen from the prominent contribution from PMMA related peaks⁴¹ compared to sp² signal from graphene (Figure 6c). On the other hand, the IPA and anthracene samples exhibited dominating graphene (sp²) contribution and traces of carboxyl (Binding energy (BE) ≈ 289 eV), methoxy (BE ≈ 287 eV) groups, and sp³ carbon (Figure 6d, e). The overall trend observed in XPS measurements agrees with SEM and

Raman results and shows significant reduction of impurity peaks upon cleaning in favor of pure sp^2 feature.

TEM study

Finally, the samples have also been examined using TEM to compare the quality of the resultant membranes at the nanoscale.

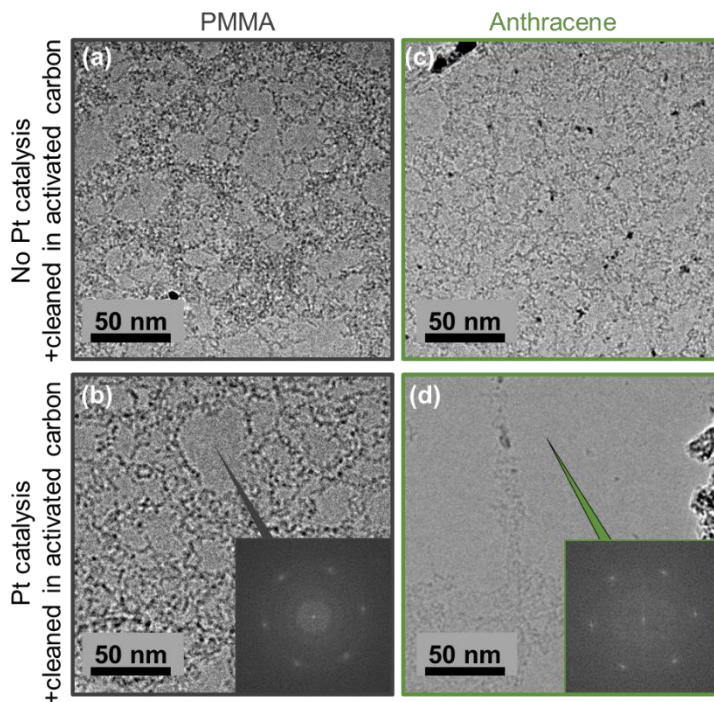


Figure 7. TEM images of graphene transferred by PMMA (a, b) and anthracene (c,d) onto a carbon mesh and treated thermally in the presence (b, d) and without (a, c) Pt catalyst. Insets are FFTs of HR TEM images ($21 \text{ nm} \times 21 \text{ nm}$) obtained from representative regions for each method (see also Figure S7).

Figures 7 a and 7 b show TEM images of the PMMA transferred graphene after final cleaning in activated carbon taken from the areas not affected by Pt catalyst (panel a) and areas in proximity to Pt catalyst (panel b). The membranes have the domains of pristine graphene and network of contaminants. The presence of the Pt catalyst results in enlargement of the area of pristine graphene, which can be as large as $\approx 2 \times 10^3 \text{ nm}^2$. The cleaning effect is even more pronounced for anthracene impurities (compare Figures 7c and d). The combined Pt and activated carbon

cleaning results in the appearance of very large patches of clean graphene with a typical area $\approx 2 \times 10^4 \text{ nm}^2$, which is comparable to or even better than previously reported results.⁴²

Conclusions

In conclusion, we present a new method of clean CVD-Gr transfer using anthracene as a sacrificial layer. It should not be seen a universal or simplest method but rather suitable for specific applications where graphene coverage is required over the chemically reactive and temperature sensitive substrates. The advantage of this approach is the dry removal of the sacrificial layer at temperatures below 150 °C, which often is a requirement for the aforementioned systems. Using high surface sensitivity of LVSEM and XPS, we compare the cleanliness of the suspended membranes transferred by different methods with the same cleaning procedures. SEM, XPS and TEM studies demonstrated the advantage of the anthracene method in combination with annealing in air in the presence of Pt catalyst followed by annealing in activated carbon to achieve a cleaner CVD-grown graphene. Note, the thermal treatment of the graphene in activated carbon has a potential drawback: after cleaning, a small amount of activated carbon dust particles adheres to the sample. Therefore, whether cleaning in activated carbon should be applied depends on the particular graphene application. We envision that our approach may be suitable in applications where dry and clean transfer protocols are required.

Corresponding Author

[*andrei.kolmakov@nist.gov](mailto:andrei.kolmakov@nist.gov)

Author Contributions

AK, AY, and MSL conceived and designed the experiments; AY, AK and GC performed the experiments and analyzed the data; IVV produced graphene samples; GC, AM and AHW characterized the samples; AY, AK, MSL, and AHW co-wrote the paper.

Acknowledgements

This work has been conducted at CNST, NIST using CNST NanoFab facilities and was supported in part by the NIST-CNST/UMD-IREAP Cooperative Agreement. MSL thanks the 2014 Minta Martin Award at UMD. The discussions and feedback from Dr. I. Levin and Dr. N. Zhitenev are greatly appreciated.

References

1. J. S. Bunch, A. M. Van Der Zande, S. S. Verbridge, I. W. Frank, D. M. Tanenbaum, J. M. Parpia, H. G. Craighead and P. L. McEuen, *Science*, 2007, **315**, 490-493.
2. F. Schedin, A. Geim, S. Morozov, E. Hill, P. Blake, M. Katsnelson and K. Novoselov, *Nature materials*, 2007, **6**, 652-655.
3. J.-N. Longchamp, T. Latychevskaia, C. Escher and H.-W. Fink, *Applied Physics Letters*, 2012, **101**, 113117.
4. J. M. Yuk, J. Park, P. Ercius, K. Kim, D. J. Hellebusch, M. F. Crommie, J. Y. Lee, A. Zettl and A. P. Alivisatos, *Science*, 2012, **336**, 61-64.
5. J. Kraus, R. Reichelt, S. Guenther, L. Gregoratti, M. Amati, M. Kiskinova, A. Yulaev, I. Vlasiouk and A. Kolmakov, *Nanoscale*, 2014, **6**, 14394-14403.
6. M. Krueger, S. Berg, D. A. Stone, E. Strelcov, D. A. Dikin, J. Kim, L. J. Cote, J. Huang and A. Kolmakov, *ACS nano*, 2011, **5**, 10047-10054.
7. J. Gu, X. Yang, Z. Lv, N. Li, C. Liang and Q. Zhang, *International Journal of Heat and Mass Transfer*, 2016, **92**, 15-22.
8. X. Li, C. W. Magnuson, A. Venugopal, R. M. Tromp, J. B. Hannon, E. M. Vogel, L. Colombo and R. S. Ruoff, *Journal of the American Chemical Society*, 2011, **133**, 2816-2819.
9. J. W. Suk, A. Kitt, C. W. Magnuson, Y. Hao, S. Ahmed, J. An, A. K. Swan, B. B. Goldberg and R. S. Ruoff, *ACS nano*, 2011, **5**, 6916-6924.
10. A. Reina, H. Son, L. Jiao, B. Fan, M. S. Dresselhaus, Z. Liu and J. Kong, *The Journal of Physical Chemistry C*, 2008, **112**, 17741-17744.
11. C. Dean, A. Young, I. Meric, C. Lee, L. Wang, S. Sorgenfrei, K. Watanabe, T. Taniguchi, P. Kim and K. Shepard, *Nature nanotechnology*, 2010, **5**, 722-726.
12. W. Regan, N. Alem, B. Alemán, B. Geng, Ç. Girit, L. Maserati, F. Wang, M. Crommie and A. Zettl, *Applied Physics Letters*, 2010, **96**, 113102.
13. Z. Cheng, Q. Zhou, C. Wang, Q. Li, C. Wang and Y. Fang, *Nano letters*, 2011, **11**, 767-771.
14. M. Ishigami, J. Chen, W. Cullen, M. Fuhrer and E. Williams, *Nano letters*, 2007, **7**, 1643-1648.

15. J. D. Wood, G. P. Doidge, E. A. Carrion, J. C. Koepke, J. A. Kaitz, I. Datye, A. Behnam, J. Hewaparakrama, B. Aruin and Y. Chen, *Nanotechnology*, 2015, **26**, 055302.
16. Y.-C. Lin, C.-C. Lu, C.-H. Yeh, C. Jin, K. Suenaga and P.-W. Chiu, *Nano letters*, 2011, **12**, 414-419.
17. P. Gupta, P. D. Dongare, S. Grover, S. Dubey, H. Mangain, A. Bhattacharya and M. M. Deshmukh, *Scientific reports*, 2014, **4**.
18. L. Gao, W. Ren, H. Xu, L. Jin, Z. Wang, T. Ma, L.-P. Ma, Z. Zhang, Q. Fu and L.-M. Peng, *Nature communications*, 2012, **3**, 699.
19. J. Kang, D. Shin, S. Bae and B. H. Hong, *Nanoscale*, 2012, **4**, 5527-5537.
20. A. V. Zaretski and D. J. Lipomi, *Nanoscale*, 2015, **7**, 9963-9969.
21. C. T. Cherian, F. Giustiniano, I. Martin-Fernandez, H. Andersen, J. Balakrishnan and B. Özyilmaz, *Small*, 2015, **11**, 189-194.
22. K. S. Kim, Y. Zhao, H. Jang, S. Y. Lee, J. M. Kim, K. S. Kim, J.-H. Ahn, P. Kim, J.-Y. Choi and B. H. Hong, *Nature*, 2009, **457**, 706-710.
23. S. Bae, H. Kim, Y. Lee, X. Xu, J.-S. Park, Y. Zheng, J. Balakrishnan, T. Lei, H. R. Kim and Y. I. Song, *Nature nanotechnology*, 2010, **5**, 574-578.
24. V. Oja and E. M. Suuberg, *Journal of Chemical & Engineering Data*, 1998, **43**, 486-492.
25. J.-N. Longchamp, C. Escher and H.-W. Fink, *Journal of Vacuum Science & Technology B*, 2013, **31**, 020605.
26. G. Algara-Siller, O. Lehtinen, A. Turchanin and U. Kaiser, *Applied Physics Letters*, 2014, **104**, 153115.
27. X. Li, W. Cai, J. An, S. Kim, J. Nah, D. Yang, R. Piner, A. Velamakanni, I. Jung and E. Tutuc, *Science*, 2009, **324**, 1312-1314.
28. I. Vlassiouk, M. Regmi, P. Fulvio, S. Dai, P. Datskos, G. Eres and S. Smirnov, *ACS Nano*, 2011, **5**, 6069-6076.
29. E. Mikmeková, H. Bouyanfif, M. Lejeune, I. Müllerová, M. Hovorka, M. Unčovský and L. Frank, *Journal of microscopy*, 2013, **251**, 123-127.
30. G. Cheng, I. Calizo and A. R. H. Walker, *Carbon*, 2015, **81**, 678-687.
31. Y. Lin and D. C. Joy, *Surface and interface analysis*, 2005, **37**, 895-900.
32. H. Demers, N. Poirier-Demers, A. R. Couture, D. Joly, M. Guilmain, N. de Jonge and D. Drouin, *Scanning*, 2011, **33**, 135-146.
33. Z. Li, Y. Wang, A. Kozbial, G. Shenoy, F. Zhou, R. McGinley, P. Ireland, B. Morganstein, A. Kunkel and S. P. Surwade, *Nature materials*, 2013, **12**, 925-931.
34. O. Cretu, A. V. Krasheninnikov, J. A. Rodríguez-Manzo, L. Sun, R. M. Nieminen and F. Banhart, *Physical review letters*, 2010, **105**, 196102.
35. P. Y. Huang, C. S. Ruiz-Vargas, A. M. van der Zande, W. S. Whitney, M. P. Levendorf, J. W. Kevek, S. Garg, J. S. Alden, C. J. Hustedt and Y. Zhu, *Nature*, 2011, **469**, 389-392.
36. X. Li, Y. Zhu, W. Cai, M. Borysiak, B. Han, D. Chen, R. D. Piner, L. Colombo and R. S. Ruoff, *Nano letters*, 2009, **9**, 4359-4363.
37. A. Pirkle, J. Chan, A. Venugopal, D. Hinojos, C. Magnuson, S. McDonnell, L. Colombo, E. Vogel, R. Ruoff and R. Wallace, *Applied Physics Letters*, 2011, **99**, 122108.
38. M. Her, R. Beams and L. Novotny, *Physics Letters A*, 2013, **377**, 1455-1458.
39. C. Fadley, R. Baird, W. Siekhaus, T. Novakov and S. Bergström, *Journal of Electron Spectroscopy and Related Phenomena*, 1974, **4**, 93-137.
40. W. Smekal, W. S. Werner and C. J. Powell, *Surface and interface analysis*, 2005, **37**, 1059-1067.
41. G. Beamson and D. Briggs, *High resolution XPS of organic polymers*, Wiley, 1992.
42. R. Zan, U. Bangert, Q. Ramasse and K. S. Novoselov, *The Journal of Physical Chemistry Letters*, 2012, **3**, 953-958.

Supplemental information for

Toward Clean Suspended CVD Graphene

Alexander Yulaev^{1,2,3}, Guangjun Cheng⁴, Angela R. Hight Walker⁴, Ivan V. Vlassiuk⁵, Aline Myers¹, Marina S. Leite^{2,6}, and Andrei Kolmakov^{1}*

¹Center for Nanoscale Science and Technology, NIST, Gaithersburg, MD 20899, USA;

²Department of Materials Science and Engineering, University of Maryland, College Park, MD 20742, USA;

³Maryland NanoCenter, University of Maryland, College Park, MD 20742, USA;

⁴Physical Measurement Laboratory, NIST, Gaithersburg, MD 20899, USA;

⁵Oak Ridge National Laboratory, Oak Ridge, TN 37831, USA;

⁶Institute for Research in Electronics and Applied Physics, University of Maryland, College Park 20742, USA

Keywords: graphene transfer, anthracene, purity, scanning electron microscopy

*To whom correspondence should be sent: andrei.kolmakov@nist.gov

Anthracene thermal evaporation

The anthracene film was deposited onto a Gr/copper stack by thermal evaporation in an evacuated glass test tube. The copper foil with CVD-grown graphene was tightly attached to the copper supporting tube. The copper tube was used for pumping of the test tube before anthracene deposition, as well as a cold finger for the substrate. In order to grow a uniform anthracene film,

the copper tube was cooled with liquid nitrogen during the anthracene deposition. The bottom part of the glass tube was filled with 1 mm size anthracene particles (purity $\geq 99\%$), pumped to $\approx 10^{-3}$ Pa, and then immersed into a boiling water bath to evaporate anthracene. After 30 min of anthracene evaporation, $14\ \mu\text{m} \pm 7\ \mu\text{m}$ thick layer of anthracene film has been deposited onto the Gr-copper specimen. To avoid water condensation onto the anthracene film upon venting, the glass tube with the sample was constantly evacuated until the temperature of the copper tube and mounted sample reached room temperature.

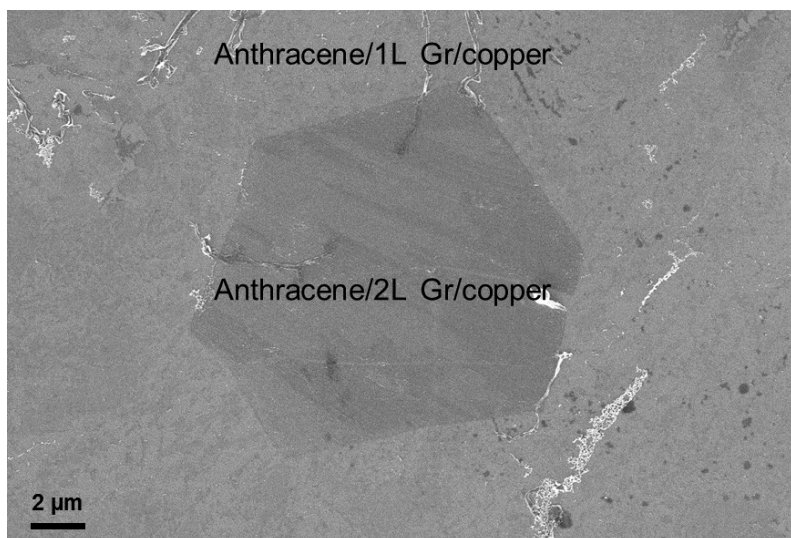


Figure S1. SEM image of an anthracene film thermally evaporated on Gr/copper at ≈ -20 °C. The hexagon in the middle of the image is the island of two-layer Gr. Both single and two-layer graphene are buried under the anthracene film. The film deposited onto a substrate at room temperature tends to form an incomplete film of weakly bound crystallites as large as few tens of μm (Figure S2). Capillary forces can easily destroy such a sacrificial layer during wet copper etching, which would make the transfer problematic.

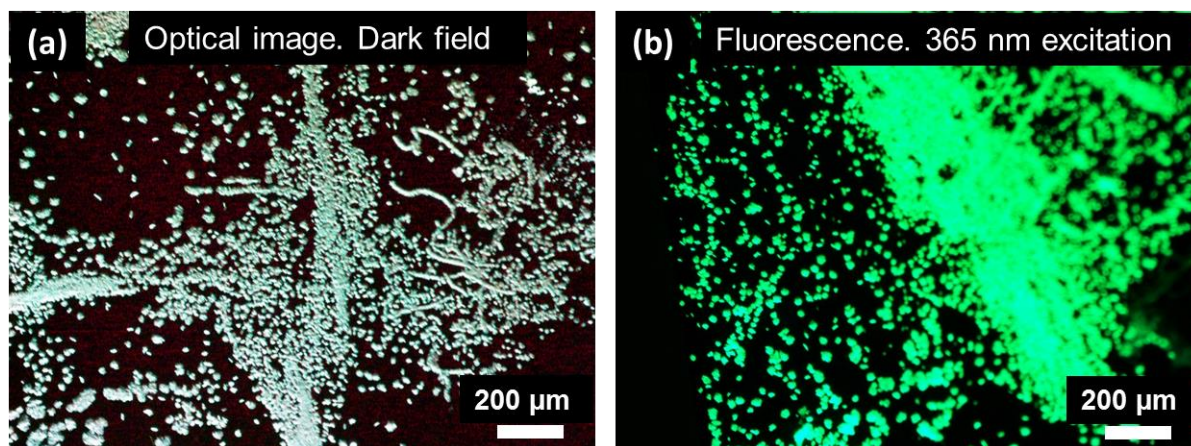


Figure S2. The morphology of the anthracene film deposited onto Gr/copper stack held at the room temperature. (a) Dark field optical image. The dark areas correspond to pristine graphene on copper. (b) Fluorescent microscopy image of the same region as in (a) excited by 365 nm UV light.

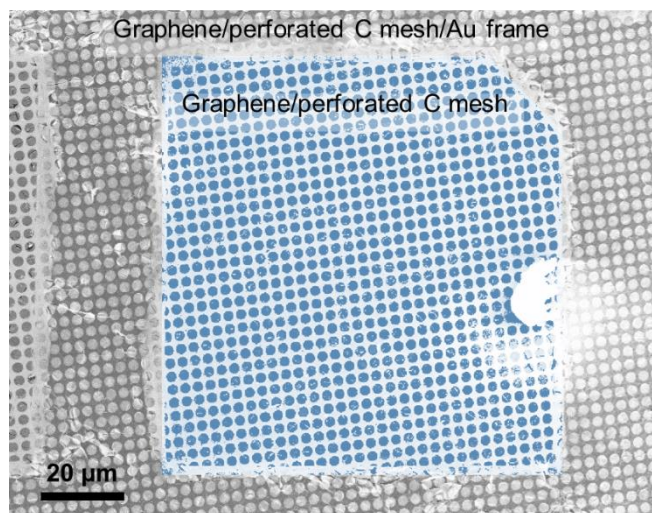


Figure S3. SEM image showing perforated carbon mesh covered with as transferred suspended graphene (false blue color) Surface coverage ($\approx 95\%$ before anthracene cleaning procedures) was calculated as the ratio of orifices covered with graphene to all orifices in carbon mesh.

Raman Characterization

Raman spectra were acquired under ambient conditions with a micro-Raman spectrometer equipped with a 514.5 nm (2.41 eV) wavelength excitation laser and a grating with a 1800 mm^{-1} pitch, while operating in 180° backscattering geometry. A $50\times$ objective was used to focus the excitation laser to an approximately $1\ \mu\text{m}$ spot onto the sample with an incident power of less than 2 mW to avoid local heating effects.

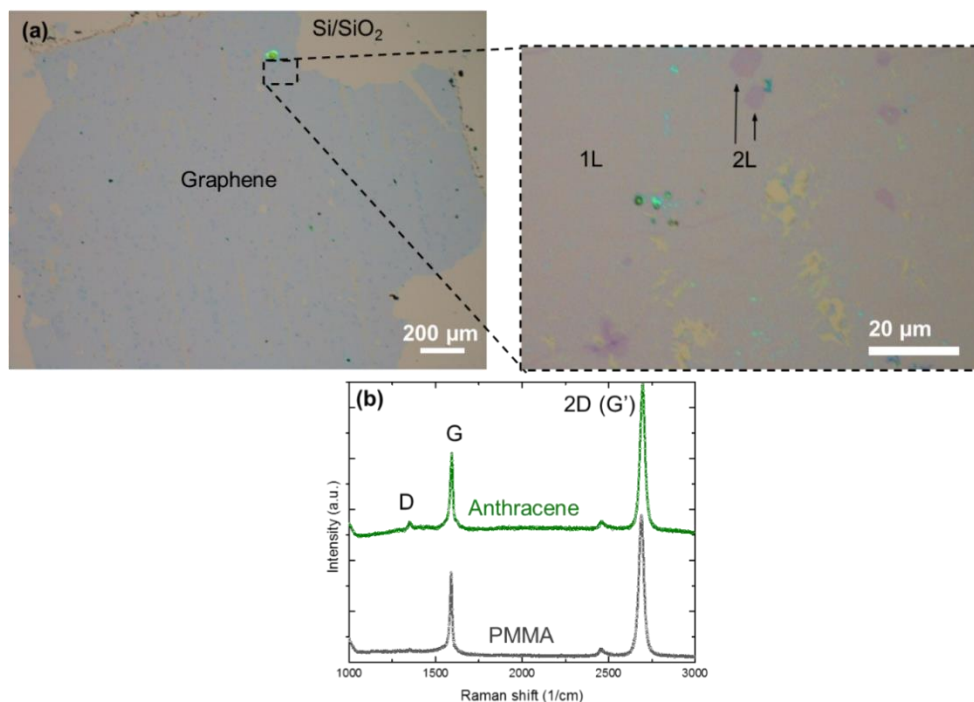


Figure S4. Optical image of graphene transferred on SiO₂ and Raman analysis. (a) Optical image of CVD Graphene transferred by anthracene onto SiO₂ (285 nm)/ Si(100) substrate (see Figure 1a, (vi)), and (b) Raman spectra of graphene transferred by PMMA and anthracene onto SiO₂ (285 nm)/Si(100) substrate. The D-peak (1360 cm⁻¹) indicates the defect density of graphene layers, the G-peak (1580 cm⁻¹) is due to Stokes phonon energy shift of the in-plane vibrational mode, and the 2D (G')-peak (2690 cm⁻¹) is the second-order overtone of another in-plane vibration. The wavelength of the excitation laser was 514.5 nm.

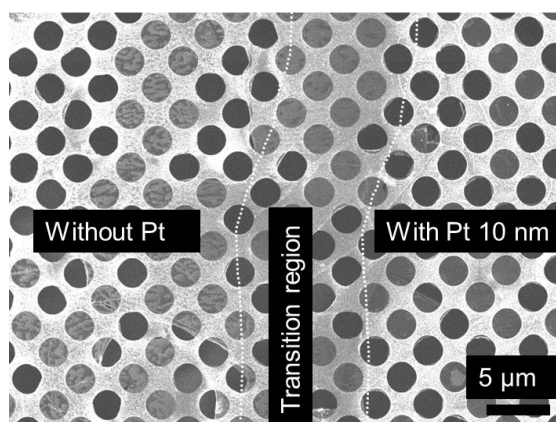


Figure S5. Spillover of Pt catalysis. SEM image of suspended graphene transferred by PMMA on a carbon mesh with a pre-deposited 10 nm Pt layer (right side) and without Pt (left side). Both the region with and without Pt are separated by a transition section (in the center) which is not covered by Pt, but represents graphene membranes cleaned by hydrogen diffused here from the Pt area.

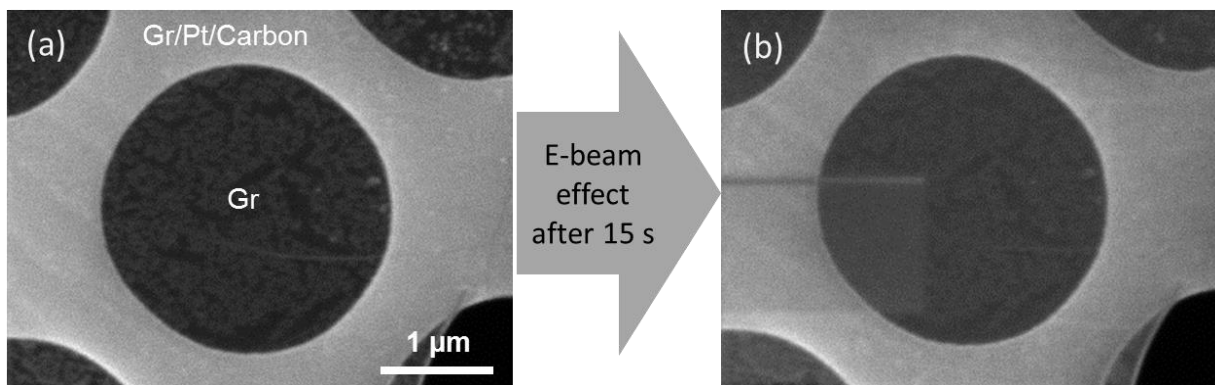


Figure S6. E-beam induced carbon contamination of a graphene membrane transferred by PMMA onto a carbon mesh with Pt and annealed on a hot plate.

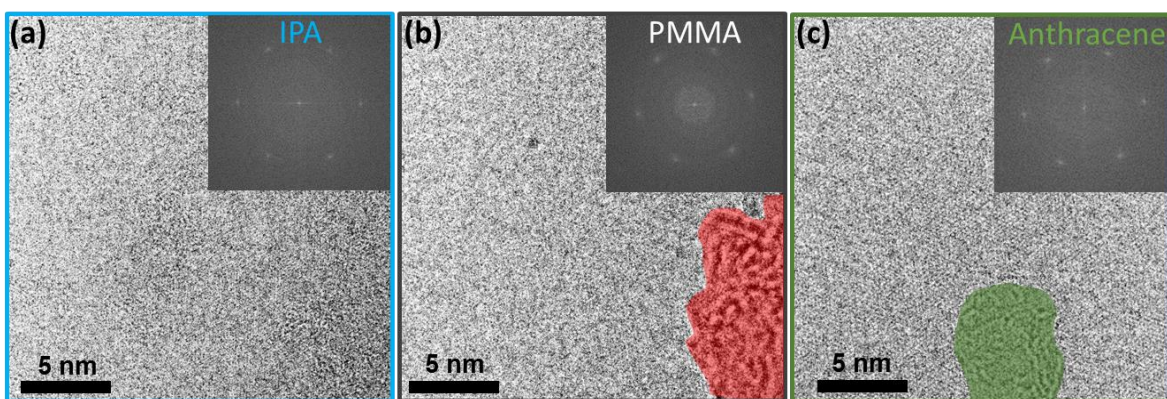
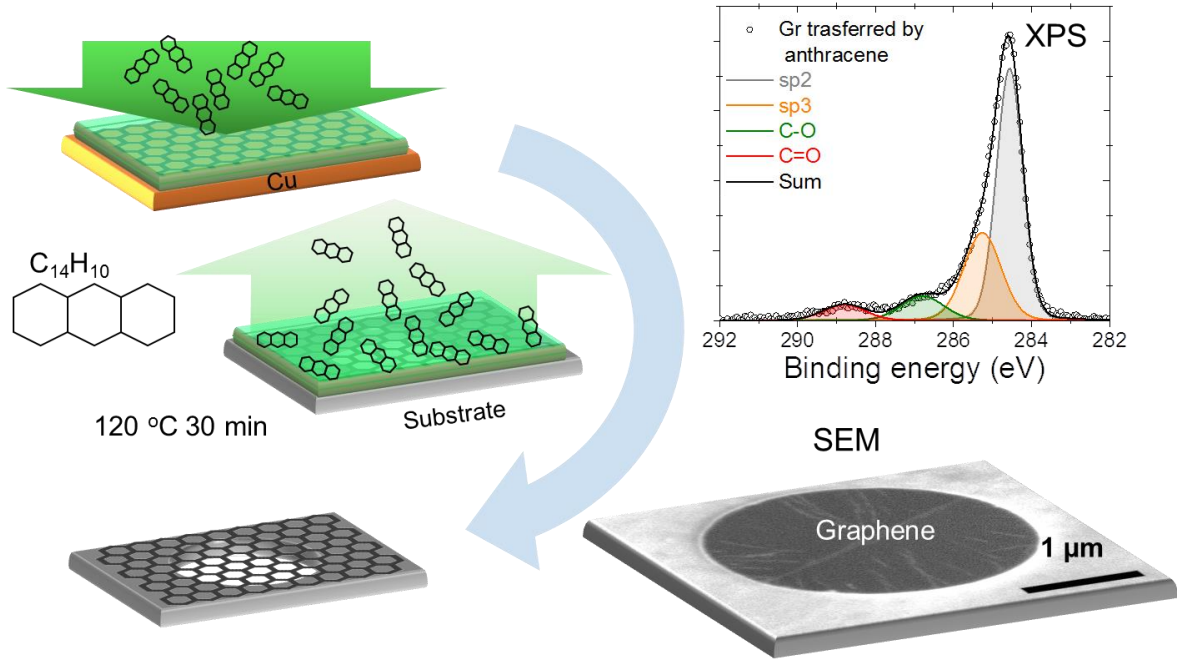


Figure S7. HRTEM images and fast Fourier transforms (FFTs) (insets) of graphene transferred by IPA (a), PMMA (b), and anthracene (c) onto a carbon mesh with Pt catalyst. Color coded regions have been excluded from FFT analysis.

TOC



Anthracene was proposed as a new easily evaporable sacrificial layer for a dry CVD graphene transfer